Journal of Alloys and Compounds 509 (2011) 1915–1919

Contents lists available at ScienceDirect

Journal of Alloys and Compounds

journal homepage: www.elsevier.com/locate/jallcom

Combustion synthesis of Co-doped zinc oxide nanoparticles using mixture of citric acid–glycine fuels

Sousan Rasouli [a,*], Shirin Jebeli Moeen [b]

[a] Department of Nanomaterials & Nanocoatings, Institute for Color Science and Technology (ICST), 55 Vafamanesh Ave., HosseinAbad Square, Pasdaran St, 1668814811, Tehran, Iran
[b] Department of Inorganic Pigments and Glaze, Institute for Color Science and Technology (ICST), 55 Vafamanesh Ave., HosseinAbad Square, Pasdaran St, 1668814811, Tehran, Iran

ARTICLE INFO

Article history:
Received 9 May 2010
Received in revised form 11 October 2010
Accepted 21 October 2010
Available online 30 October 2010

Keywords:
Chemical synthesis
Nanostructured materials
Co:ZnO
Color properties

ABSTRACT

In this study, cobalt-doped ZnO nanoparticles were synthesized by combustion method. Mixtures of citric acid and glycine were used as fuel. As-prepared powders were characterized by XRD, XPS, SEM-EDX, TEM and spectrophotometer. XRD patterns indicated that combustion reaction by different fuel mixture resulted in the formation of pure ZnO phase. However, citric acid combustion alone led to amorphous powder. Scherrer's equation demonstrated that the crystallite size increases with citric acid/glycine (C/G) ratio (38–61 nm). SEM and TEM images illustrated that the morphology of the powder depends on the C/G ratios and changes from rod-like to spongy hexagonal particles. Reflectance spectra showed that by higher C/G ratios, deeper green colors are obtained.

1. Introduction

There has been increasing interest in ZnO nanostructures due to their variety of morphologies and availability of simple and low cost processing. Moreover, ZnO remains as a dominant material which holds great promise for a variety of applications such as varistors and surface acoustic wave devices, and future applications, including UV light-emitting diodes and transparent field-effect transistors [1,2]. ZnO can be ferromagnetic by doping with transition metals such as Mn, Fe, Cr, Co and V, the materials would be suitable for a number of devices such as spin field emission transistors (FETs), and light emitting diodes (LEDs) with circularly polarized light emission [3]. Moreover, Co:ZnO nanopowders show ferromagnetic properties even at room temperature [4–6].

Synthesis of Co:ZnO nanoparticles is an area of interest research. Co doped with ZnO has been synthesized via sol–gel [7], hydrothermal [8], wet chemical [9,10] and precipitation methods [11]. However, Co doped ZnO nanoparticles could be prepared by fast, simple and inexpensive solution combustion method [12]. Ching Hwang et al. and Rao et al. synthesized ZnO and Co:ZnO nanoparticles by auto-combustion using glycine as fuel [13,14]. Other fuels are also investigated. Ekambaram et al. showed solution combustion of transition metal-incorporated ZnO particles using 3-methylpyrazole-5-one (3MP5O) as a fuel [15]. Sharma et al. reported synthesis of ZnO powders via dry combustion rout using different urea/oxidizer ratios [16].

Major parameters such as fuel type, fuel mixture and fuel/oxidizer ratio can play an important role on phase formation of different compounds. Li et al. showed that because of formation of amorphous materials, citric acid is not an effective fuel by itself. Moreover, when citric acid is used, no precipitation happens during combustion process because of stronger complexing ability of citric acid [17]. All amine group-contained fuels decompose at relatively low temperatures [18]. Accordingly, an appropriate mixture of citric acid and glycine would be the best choice to use both of the complexing ability of citric acid and the combustion nature of glycine [19].

To our knowledge, the effect of fuel on phase formation, morphology and size of ZnO and transition metal doped ZnO has not reported yet. In this study, the effect of citric acid and glycine as well as their mixtures on phase formation, morphology, and particle size as well as color characteristics is investigated.

2. Experimental details

All materials used in this study were of analytical grade. Previous work has demonstrated that for solid state reaction a complete solid solution of Co:ZnO can be achieved by addition of 0–20 wt% of Co_3O_4 [11]. Since low amounts of cobalt (less than 5%) are not detectable by XRD technique, 10 wt% Co was used to insure complete formation of solid solution. In this case, $Zn_{0.9}Co_{0.1}O$ was considered as the stoichiometric composition.

* Corresponding author. Tel.: +98 21 229 52272; fax: +98 21 229 47537.
E-mail address: rasouli@icrc.ac.ir (S. Rasouli).

0925-8388/$ – see front matter © 2010 Elsevier B.V. All rights reserved.
doi:10.1016/j.jallcom.2010.10.087

Table 1
Synthesized samples with different amounts of citric acid and glycine fuels.

Sample	Citric acid, %	Glycine, %
C100G0	100	0
C75G25	75	25
C50G50	50	50
C25G75	25	75
C0G100	0	100

The exothermic redox stoichiometric reactions between oxidizer (zinc nitrate) and fuels (glycine or citric acid) to achieve $Zn_{0.9}Co_{0.1}O$ composition can be expressed as follows:

$$0.9Zn(NO_3)_2 \cdot 6H_2O + 0.1Co(NO_3)_2 \cdot 6H_2O + \psi NH_2CH_2COOH \rightarrow Zn_{0.9}Co_{0.1}O + 6\psi CO_2 + 7.9\psi H_2O + 0.95\psi N_2 \quad (1)$$

$$0.9Zn(NO_3)_2 \cdot 6H_2O + 0.1Co(NO_3)_2 \cdot 6H_2O + \psi C_6H_8O_7 \rightarrow Zn_{0.9}Co_{0.1}O + 6\psi CO_2 + (4\psi + 6)H_2O + N_2 \quad (2)$$

where the Ψ represents the ratio at which the value of oxygen balance is equal to zero. This F/O (fuel/oxidizer) ratio reaches to 10/9 for glycine (reaction (1)) and 5/9 for citric acid (reaction (2)) fuels [20].

In the case of fuel mixtures, the fuel composition was calculated by molar ratios between Citric acid/Glycine (C/G) fuels. As a typical example, stoichiometric amounts of $Zn(NO_3)\cdot 6H_2O$ and $Co(NO_3)_2\cdot 6H_2O$ dissolved completely in deionized water into beaker vessel. Then, mixture of fuels was slowly introduced to solution under vigorous stirring and the temperature increased up to 90 °C. After 30 min, the solution completely converted to a highly viscous gel. Next, the beaker vessel was transferred into microwave oven to complete the combustion reaction after about 50 s. The synthesized samples are listed in Table 1.

The obtained powders were characterized by X-ray diffraction using a D-500 (Siemens, Karlsruhe, Germany) diffractometer. Size and morphology of the samples were observed by LEO 1455 VP scanning electron microscope (SEM) and transition electron microscopy (TEM). The elemental distribution of samples was determined with an attached energy dispersion X-ray spectrometer (EDX, Oxford Instruments). Color properties of the obtained products were determined by Ultraviolet radiation spectroscopy in the visible–ultraviolet light region. Diffuse reflectance was determined with a Color Eye 7000A spectrometer in the range between 300 and 700 nm.

3. Results and discussion

3.1. Crystal structures of synthesized samples

Fig. 1 shows the XRD patterns of as synthesized powders obtained by different fuel ratios. It can be observed that very intense single hexagonal ZnO phase with P63mc structure (JCPDS 5-664) was obtained except for C100G0 which amorphous phase is observed. Moreover, in the case of C100G0, the extremely broad peaks at about 32° and 36° are indicative of nano-crystalline nature of the ZnO phase. According to the patterns, the peak intensity of ZnO phase increases with glycine content. This observation can be due to the decomposition of glycine which occurs at lower temperatures in comparison with citric acid. Li et al. [18] illustrated this phenomenon in the case of synthesis of γ-lithium aluminate using various fuels. So, the energy released from redox reaction of glycine fuel, zinc and cobalt nitrate accelerates the phase formation of ZnO.

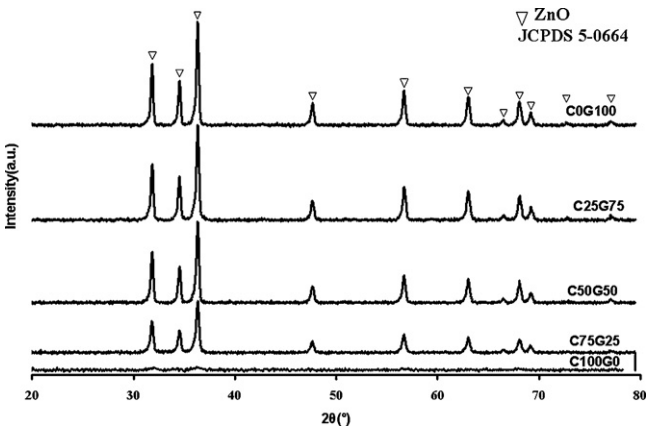

Fig. 1. XRD diffraction patterns of Co:ZnO powders synthesized using different fuel mixtures (C100G0, C75G25, C50G50, C25G75 and C0G100 samples).

The average crystallite size (D) was determined by Debye–Scherrer's formula according to Eq. (3):

$$D = \frac{0.9\lambda}{\beta \cos\theta} \quad (3)$$

where λ is the wavelength of incident X-ray, β is the half width of diffracted peak and θ is diffracted angle. The trend of average crystallite size as a function of fuel mixture ratio is illustrated in Fig. 2 in which the average crystallite size increases with glycine content from 37 to 63 nm. In fact, auto-combustion of glycine releases more energy than citric acid, which can lead to rapid crystal growth.

3.2. The oxidation state of cobalt in ZnO structure

XPS survey spectra obtained from C0G100 sample are shown in Fig. 3(a) in which, all peaks are related to Zn–O–Co bonds. Two weak peaks appear at 765–800 eV, corresponding to Co $2p_{3/2}$ and Co $2p_{1/2}$. High resolution spectrum of Co 2p bonding energy region is illustrated in Fig. 3(b). The curve fitted on spectrum reveals the appearance of Co $2p_{3/2}$ peak at 781.8 eV and Co $2p_{1/2}$ at 798 eV. S.H. Ha et al. [21] showed that the position of Co $2p_{3/2}$ peak is related to the change of oxidation state of Co element. Therefore, the Co $2p_{3/2}$ peak at 781 eV is related to Co with its 2^+ oxidation state. Moreover, the energy difference between Co $2p_{3/2}$ and Co $2p_{1/2}$ is near to 15.5, which indicates the existence of Co^{2+} in $Zn_{0.9}Co_{0.1}O$ structure [22].

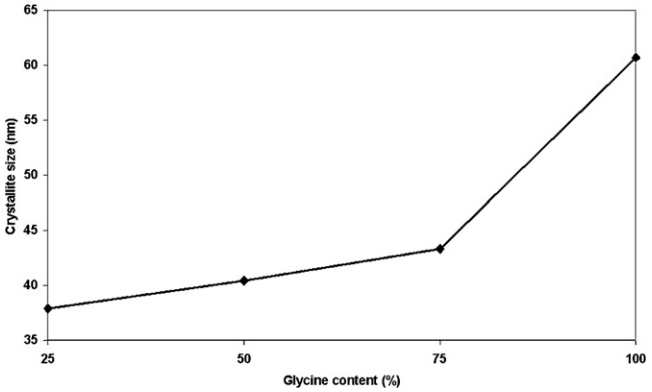

Fig. 2. Crystallite size of different citric acid–glycine content samples synthesized by auto-combustion method.

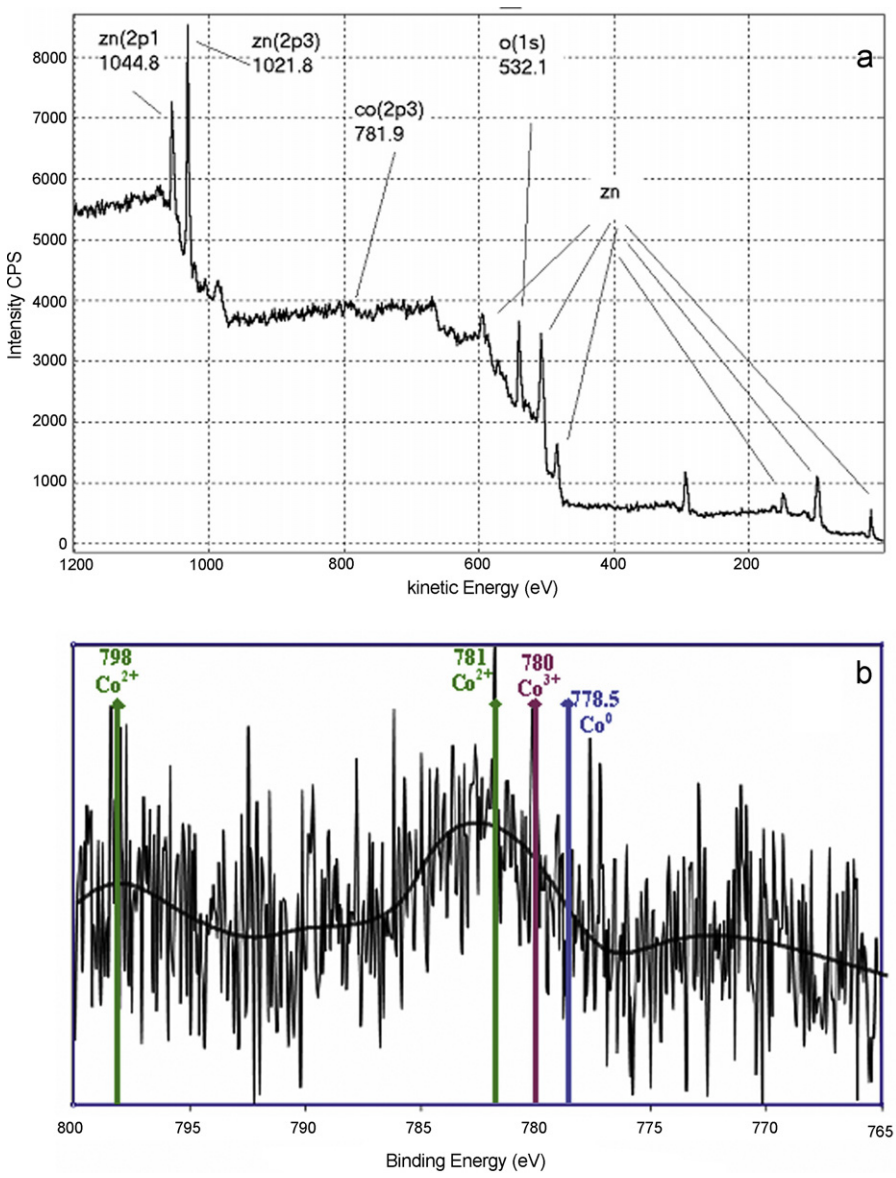

Fig. 3. (a) XPS spectrum of C0G100 sample and (b) high resolution of Co $2p_{3/2}$ and $2p_{1/2}$ region.

3.3. *The microstructures of synthesized samples*

Fig. 4 shows the SEM images of Co:ZnO powders obtained by different fuel mixture ratios. As shown in Fig. 4(a), C75G25 powder consists of semispherical loosely agglomerated particles. This morphology is due to the inherent effect of the organic fuels [23]. Citric acid has more effective complexing role than glycine, because of the chelating effect [24]. Subsequently, the powder synthesized in the presence of higher content of citric acid has finer particles with uniform size. Moreover, Fig. 3(a)–(d) shows that the size and morphology of obtained powders have been changed by increasing glycine content. In fact, the released energy from combustion reaction is associated with enhancement of amine groups as a result of glycine enrichment [18]. When the ignition of metal nitrate starts in the presence of nitrogen-based fuels, localization of heat on the particle boundaries results in semi-sintered particles [25] observed in Fig. 4(b) and (c). Furthermore, the increasing of localized heat with glycine content leads to rapid crystal growth. The increase of particle size in Fig. 4(b) and (c) in comparison with Fig. 4(a) is in good agreement with crystallite size results in Fig. 2. In the case of C0G100, formation of porous spongy morphology is observed which is related to larger amount of exhaust gas release from combustion reaction.

The elemental distribution of C0G100 was determined with EDX analysis. From Fig. 5, the EDX spectrum shows only the presence of Co, Zn and oxygen which is in agreement with the results from XPS in Fig. 3. Moreover, the atomic percent of Co^{2+} in the synthesized powder is about 4.5%.

TEM images of Co:ZnO powders synthesized by different fuel mixtures are shown in Fig. 6. Combustion in the presence of citric acid leads to the formation of fine rod-like nanoparticles (Fig. 6(a)). However, in these conditions, structure mainly consists of amorphous phase. As shown in Fig. 6(b) and (c), particle size increases from 200 to 300 nm with glycine content. Wu et al. [24] illustrated that using glycine as fuel, larger particles with better crystallinity can be obtained. In Fig. 6(c) and (d), the higher energy released from glycine causes the formation of semi-sintered particles. Higher amounts of exhaust gases lead to the formation of loose packing agglomerates which in turn causes more pore/particle ratio.

From Figs. 4 and 6, it seems that three different morphologies concerning the kind of fuel are obtained in C100G0 to C0G100 samples. The first is rod like morphology appeared in sample

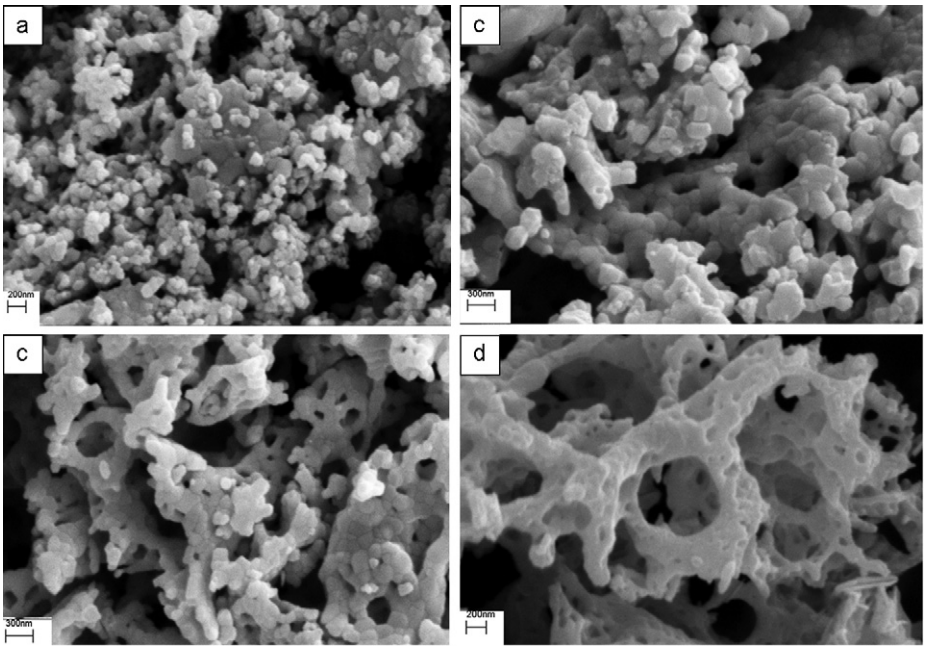

Fig. 4. SEM images of samples combustion synthesized using different fuel mixtures: (a) C75G25, (b) C50G50, (c) C25G75 and (d) C0G100 samples.

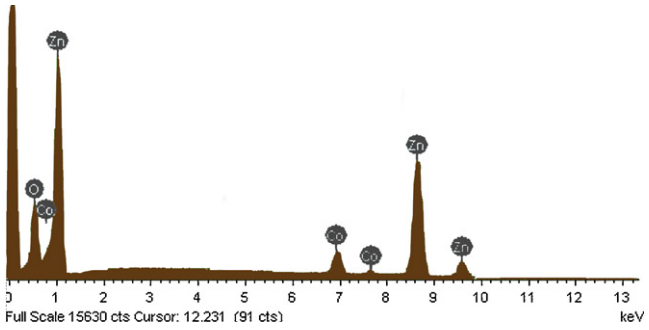

Fig. 5. The elemental distribution of sample C0G100 determined with energy dispersion X-ray spectrometer EDX.

C100G0 (pure citric acid fuel). Rod-like structure of ZnO nanoparticle can be related to carboxylic groups of citric acid. Yang et al. [26] showed that the adsorption of growth units on crystal surfaces strongly affects the growth speed and the orientation of the crystals. Hence, adsorption of citric acid carboxylic groups on the crystal surface can influence the orientation and morphology of the particles [27]. The complex of citric acid and Zn ions in the precursor tends to be perpendicular to the absorbed surface. After combustion reaction, the growth units would tend to face-land onto the growing interface. Therefore, different growth rate of crystal plane causes rod-like growth of ZnO structure [26].

The second morphology is spherical polycrystalline aggregates or semi-spherical particles appeared in C75G25 and C50G50 samples due to radiating growth from the center [16]. The third kind is platelet morphology with large pores and high surface area which was observed in C25G75 and C0G100 samples and is probably due to the evolution of large amount of gases as by-products [16]. Strong agglomeration is observed in the two latter morphologies. Since high flame temperature of glycine fuel results in the formation of semi-sintered nanoparticles, the resultant large agglomerates have higher resistance to dispersion by ultrasonic agitation [25].

Table 2
CIELAB coordination of Co:ZnO sample prepared by combustion in presence of different fuel mixtures.

	L^*	a^*	b^*	C^*	h
C75G25	40.776	−11.545	7.4419	13.736	147.19
C50G50	35.834	−18.85	8.31	20.6	156.21
C25G75	49.954	−26.441	10.439	28.428	158.46
C0G100	62.24	−18.31	7.68	19.85	157.25

3.4. Color properties of synthesized samples

Color properties of the synthesized samples in the presence of different fuel mixtures have been investigated using the CIELAB coordinates and spectral reflectance. In CIE $L^*a^*b^*$ color space, L^* is the lightness axis, b^* shows the color varying from blue to yellow, a^* represents the color varying from green to red. Fig. 7 shows the diffuse reflectance spectra of the as-synthesized powders. A broad reflection band around 530 nm can be observed for all samples being a characteristic peak for green region. However, the peak intensity is bigger for C0G100 meaning a lighter green color. Increase of reflectance intensity with glycine content of fuel mixtures is shown in Fig. 7. It seems that deeper green color of sample synthesized using glycine rich fuel (C75G25 and C0G100 samples) is due to good crystallinity and better substitution of Co atom in wurtzite structure. The best method for investigating the color quality of a pigment is the evaluation of pigment's chroma (C^*) and hue angle (h). C^* and h are defined as follows [28]:

$$C^*_{ab} = \{(a^*)^2 + (b^*)^2\}^{1/2} \quad (4)$$

$$h_{ab} = \tan^{-1}\left(\frac{b^*}{a^*}\right) \quad (5)$$

where a^* and b^* is the color-opponent dimensions.

Table 2 presents color properties as a function of the fuel mixtures.

In accordance with Fig. 7 and Table 2, the samples contained higher amounts of glycine (C50G50, C25G75 and C0G100) have higher a^* and L^* compared to other samples. This confirms that depending on fuel mixture, different color properties were obtained which can be well related to the crystal structure, powder

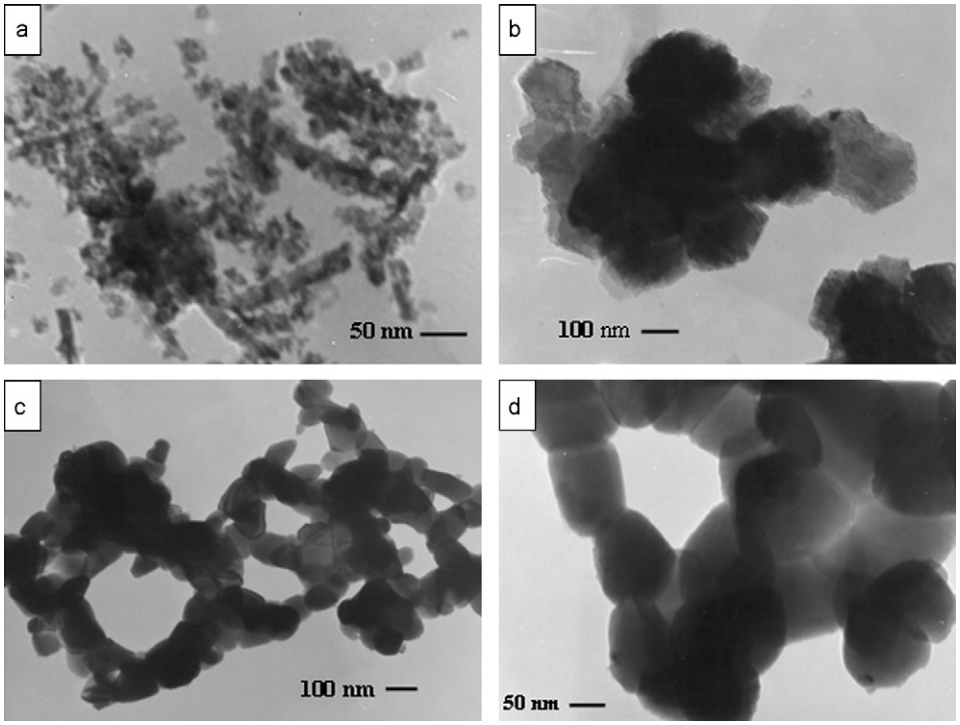

Fig. 6. TEM images of samples combustion synthesized using different fuel mixtures: (a) C100G0, (b) C75G25, (c) C50G50 and (d) C25G75 samples.

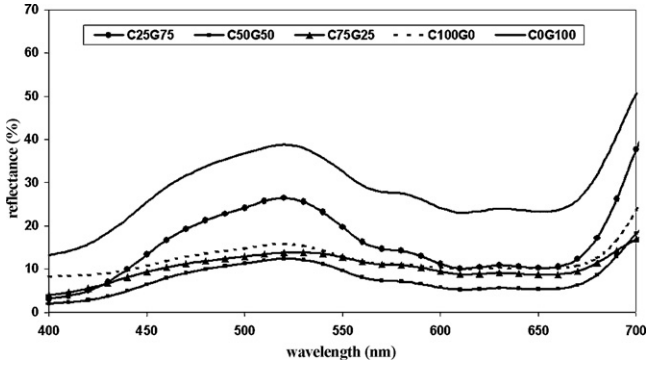

Fig. 7. The diffuse reflectance spectra of the samples synthesized using different fuel mixtures.

morphology and particle agglomeration. From C^* and h parameters, it is concluded that C0G100 and C25G75 samples have more chromaticity and has a dipper green color. Cunha et al. [29] showed that deep green color of $Zn_{0.9}Co_{0.1}O$ pigment was obtained only for a complete entrance of Cobalt into ZnO structure. They have reported this observation through investigating the effect of calcination temperature on the color of the samples due to the complete or partially entrance of Cobalt into ZnO structure.

4. Conclusions

Cobalt-doped ZnO nanocrystalline green pigments have been synthesized via combustion method in the presence of different ratios of glycine and citric acid. The crystallite size increases from 37 to 63 nm with glycine content. The morphology of synthesized powders changes as a function of fuel ratio. For example, the rod-like morphology of particles changes to spongy semi-sphere by increasing the glycine content. Spongy semi-sintered particles form due to high glycine content in fuel mixtures. Deeper green color with respect to higher C^*, h and intense green reflectance (530 nm) was obtained by higher amount of glycine content in the fuel mixtures.

References

[1] D.C. look, in: C. Jagadish, S. Pearton (Eds.), Zinc Oxide Bulk, Thin Films and Nanostructures, Elsevier, Netherlands, 2006, pp. 21–42.
[2] A.B. Djurisic, A.M.C. Ng, X.Y. Chen, Prog. Quant. Electron. 34 (2010) 191–259.
[3] H. Morkoç, Ü. Özgür, Zinc Oxide Fundamentals, Materials and Device Technology, WILEY-VCH Verlag GmbH & Co. KGaA, Weinheim, 2009.
[4] J. Ma, W. Hao, R. Luo, H. Xu, Mater. Lett. 62 (2008) 403–406.
[5] C.J. Cong, J.H. Hong, K.L. Zhang, Mater. Chem. Phys. 113 (2009) 435–440.
[6] X. Zhou, S. Ge, D. Yao, y. Zuo, Y. Xiao, J. Alloys Compd. 463 (2008) L9–L11.
[7] J.H. Yang, L.Y. Zhao, Y.J. Zhang, Y.X. Wang, H.L. Liu, J. Alloys Compd. 473 (2009) 543–545.
[8] X. Xu, C. Cao, J. Alloys Compd. 501 (2010) 265–268.
[9] P. Lommens, P.F. Smet, C.D. Donega, A. Meijerink, L. Piraux, S. Michotte, S. fi-Tempfli, D. Poelman, Z. Hens, Luminescence 118 (2006) 245–250.
[10] N. Volbers, H. Zhou, C. Knies, D. Pfisterer, J. Sann, D.M. Hofmann, B.K. Meyer, Appl. Phys. A 88 (2007) 153–155.
[11] C. Rath, S. Singh, P. Mallick, D. Pandey, N.P. Lalla, N.C. Mishra, Ind. J. Phys. 83 (4) (2009) 415–421.
[12] M.L. Dinesha, H.S. Jayanna, S. Mohanty, S. Ravi, J. Alloys Compd. 490 (2010) 618–623.
[13] C. Lin, C. Hwang, W. Lee, W. Tong, Mater. Sci. Eng. B 140 (2007) 31–37.
[14] L.B. Duan, G.H. Rao, J. Yu, Y.C. Wang, Solid State Commun. 145 (2008) 525–528.
[15] S. Ekambaram, Y. Iikubo, A. Kudo, J. Alloys Compd. 433 (2007) 237–240.
[16] S.K. Sharma, S.S. Pitale, M.M. Malik, R.N. Dubey, M.S. Qureshi, S. Ojha, Physica B 405 (2010) 866–874.
[17] P. Blennow, K.K. Hansen, L.R. Wallenberg, M. Mogensen, J. Eur. Ceram. Soc. 27 (2007) 3609–3612.
[18] F. Li, K. Hu, J. Li, D. Zhang, G. Chen, J. Nucl. Mater. 300 (2002) 82–88.
[19] S. Verma, S.D. Pradhan, R. Pasricha, S.R. Sainkar, P.A. Joy, J. Am. Ceram. Soc. 88 (2005) 2597–2599.
[20] C.S. Lin, C.C. Hwang, W.H. Lee, W.Y. Tong, Mater. Sci. Eng. B 140 (2007) 31–37.
[21] S.S.Y. Lin, D.H. Kim, M.H. Engelhard, S.Y. Ha, J. Catal. 273 (2010) 229–235.
[22] S. Deka, P.A. Joy, Solid State Commun. 134 (2005) 665–669.
[23] R.V. Mangalaraja, J. Mouzon, P. Hedström, C.P. Camurri, S. Ananthakumar, M. Odén, Powder Technol. 191 (2009) 309–314.
[24] K.H. Wu, T.H. Ting, M.C. Li, W.D. Ho, J. Magn. Magn. Mater. 298 (2006) 25–32.
[25] M. Kottaisamy, D. Jeyakumar, R. Jagannathan, M. Mohan Rao, Mater. Res. Bull. 31 (1996) 1013–1020.
[26] Z. Yang, Q.-H. Liu, L. Yang, Mater. Res. Bull. 42 (2007) 221–227.
[27] Y. Liu, C-y. Liu, Z-y. Zhang, Chem. Eng. J. 138 (2008) 596–601.
[28] A.E. Lavat, C.C. Wagner, J.E. Tasca, Ceram. Int. 34 (2008) 2147–2153.
[29] J.D. Cunha, D.M.A. Melo, A.E. Martinelli, M.A.F. Melo, I. Maia, S.D. Cunha, Dyes Pigments 65 (2005) 11–14.